

A Microporous Gel Polymer Electrolyte with High Mg²⁺ Ionic Conductivity at Room Temperature

Jiawei Liu,^[a] Yigang Yan,^[b] Filicia Wicaksana,^[a] and Shanghai Wei*^[a]

Rechargeable magnesium batteries have attracted much attention due to the high theoretical volumetric capacity, abundance, and safety. However, solid-state Mg batteries have been rarely studied because of limited choices of solid-state electrolyte materials. In this research, poly(vinylidene fluoride)/poly(propylene carbonate) (PVDF/PPC) as matrix were prepared using a simple solution casting method. Ethylene carbonate (EC), diethyl carbonate (DEC), and magnesium(II) bis(trifluoromethanesulfonyl) imide [Mg(TFSI)₂] were selected to prepare liquid electrolyte. A classification of novel gel polymer electrolytes (GPEs), PVDF/PPC/Mg(TFSI)₂, was synthesized and

investigated. The electrochemical measurements show that PVDF/PPC/Mg(TFSI)₂ polymer electrolytes exhibit a high ionic conductivity, close to 10⁻² S cm⁻¹, at room temperature. The electrochemical stability window of PVDF/PPC-based GPE was up to 3 V (versus Mg²⁺/Mg). Materials characterization shows that these GPEs have a porous structure, providing a pathway for magnesium ion transport. Thermal analysis and crystal structure results indicate that PVDF crystallinity was affected by the addition of PPC. Additionally, the ion transport mechanism in the gel polymer electrolyte has been discussed.

1. Introduction

Lithium-ion batteries (LIBs) have been widely used in energy storage areas, such as electric vehicles and portable electronics.^[1] However, safety concerns, high costs, and issues related to energy density have promoted the exploration of alternative energy-storage technologies.^[2] Magnesium boosts a relatively high theoretical volumetric capacity of 3833 mAh cm⁻³, a low electrochemical potential of -2.37 V (vs. SHE), abundance on earth, a high specific capacity of 2205 mAh g⁻¹, non-toxic, and environmentally friendliness.^[3] Consequently, magnesium-ion rechargeable batteries (MRBs) are being considered as the next-generation electrical energy storage technology for industry application.^[4] However, the development of MRB faces challenges due to the limited choice of electrode materials and the search for suitable electrolytes.

Currently, liquid electrolytes for rechargeable magnesium-ion batteries mainly consist of Grignard electrolytes, magnesium borohydride-based electrolytes, and ionic liquid electrolytes.^[5] However, these organic liquid electrolytes present issues, such as low solubility, slow Mg deposition kinetics, and safety concerns.^[6] Solid-state electrolytes have garnered significant

attention in recent studies, particularly for sodium and lithium batteries, with the goal of developing high-energy density batteries with enhanced safety. Solid-state electrolytes can be categorized into inorganic-based electrolytes and polymer-based electrolytes.^[6-7] Inorganic-based electrolytes have high resistance at the electrode-electrolyte interface due to the small contact area. Flexible polymer electrolytes can overcome this limitation. Solid-state polymer-based electrolytes can be further divided into all solid-state polymer electrolytes (SPEs) and gel polymer electrolytes (GPEs). GPEs are considered promising candidates due to their low risk of electrolyte leakage and higher ionic conductivity, >10⁻³ S cm⁻¹, which is over ten times higher than that of SPEs.^[8]

Several methods exist for preparing polymer electrolytes, including solution casting, phase inversion, hot press, and cross-linking.^[7b,9] The solution casting method is a straightforward and efficient strategy for preparing polymer electrolytes, offering advantages such as ease of fabrication, flexibility, and good mechanical properties.^[6-7] So far, various polymers, including poly(ethylene oxide) (PEO),^[7b,10] poly(vinylidene fluoride) (PVDF),^[11] poly(vinylidene fluoride-co-hexafluoropropylene) (PVDF-HFP),^[9c,d, 12] polyacrylonitrile (PAN),^[13] and polytetrahydrofuran (PTHF), and poly(methyl methacrylate) (PMMA),^[9a,14] have been studied as matrices for polymer electrolytes. PVDF, widely studied in the polymer electrolytes, contains -C-F groups with fluorine atoms, resulting in a high dielectric constant ($\epsilon = 8.4$).^[15] The high dielectric constant contributes to a high degree of salt dissociation, a high charge carrier concentration, and anodic stability due to strong electron-withdrawing group. PVDF also offers superior thermal stability and decent mechanic strength. However, its tendency to crystallize is not conductive to ion transport in the polymer matrix, leading to low ionic conductivity at room temperature. Poly(propylene carbonate) (PPC) is a biodegradable and environmentally friendly polymer prepared from propylene oxide

[a] J. Liu, F. Wicaksana, S. Wei

Department of Chemical & Materials Engineering, Faculty of Engineering, The University of Auckland 1010, Auckland, New Zealand

Tel.: +64 9 9239184

Fax: +64 9 3737463

E-mail: s.wei@uckland.ac.nz

[b] Y. Yan

Institute of New Energy and Low-Carbon Technology, Sichuan University, Chengdu 610065, China

© 2024 The Authors. Batteries & Supercaps published by Wiley-VCH GmbH.

This is an open access article under the terms of the Creative Commons Attribution License, which permits use, distribution and reproduction in any medium, provided the original work is properly cited.

(PO) and carbon dioxide (CO_2). While PPC has been studied as a polymer-based electrolyte for lithium solid-state batteries,^[16] there is limited research on PPC as gel polymer electrolytes for rechargeable magnesium-ion batteries.

Liquid electrolytes can be divided into Grignard reagents, boron-based electrolytes, and inorganic electrolytes.^[7a] Grignard-based electrolytes enable reversible Mg stripping and plating. However, this system is hard to match the electrophilic positive electrode due to nucleophilic anions. Organoboron magnesium salt has been widely studied to avoid electrode corrosion caused by chloride ions. $\text{Mg}(\text{CB}_{11}\text{H}_{12})_2$ is a non-corrosive electrolyte with high voltage. However, its synthesis process is complicated.^[4a] Thus, scientists replace AlCl_3 with magnesium(II) bis(trifluoromethanesulfonyl) imide $[\text{Mg}(\text{TFSI})_2]$ to avoid corrosive.^[5] $\text{Mg}(\text{TFSI})_2$ owns high lattice energy, and is easy to dissociate with Mg^{2+} and TFSI^- anion. Liquid solvents have two classifications: polar reagents, such as nitriles, esters and carbonate, and nonpolar reagent, like ethers.^[7a] Conventional carbonate electrolytes are widely used in the liquid electrolyte. In this paper, ethylene carbonate (EC) and diethyl carbonate (DEC) are chosen to be the solvents for preparing liquid electrolyte.

PPC contains a polar ester group in the polymer chain, which is beneficial for ionic conduction by coordinating magnesium salts. It is an amorphous aliphatic polycarbonate with a relatively low glass transition temperature (T_g). The chain's relaxation and segmental motion are favorable for ion transport. However, PPC has low mechanical strength and is prone to breakage as polymer electrolytes, hindering its practical application in the battery system. To address this issue, PPC was blended with PVDF using the solution casting technique. The impact of the PPC ratio on the properties of PVDF, including porous structure, morphology, and crystallography, was systematically studied in this research. The ionic conductivity, ion transport mechanism, and electrochemical performance of different PVDF/PPC/Mg(TFSI)₂ gel polymer electrolytes for MRBs have also been discussed.

Experimental Section

Electrolyte Preparation

The blended polymer electrolytes were prepared using solution casting method. Two types of polymers, polyvinylidene difluoride (PVDF) ($M_w = 534,000$) and polypropylene carbonate (PPC) ($M_n \sim 50,000$), were first dried. Subsequently, PVDF and PPC were mixed in various mass ratios (100:0, 90:10, 80:20, 70:30, 60:40, 50:50, w/w) in an organic solvent mixture of dimethyl formamide (DMF) and acetone in a 1:1 volume ratio. The mixture was stirred overnight with a magnetic stirrer at room temperature, maintaining a concentration of 10 wt%, to form a homogenous viscous solution. The resulting solutions were then poured into a glass Petri dish and dried in an oven at 60 °C for 10 h to obtain thin polymer matrix membranes. To create the gel polymer electrolytes (GPEs), these membranes were immersed in a liquid magnesium solution (1.0 M Magnesium bis(trifluoromethanesulfonimide) $[\text{Mg}(\text{TFSI})_2]$ in ethylene carbonate (EC)/diethyl carbonate (DEC) (1:1, v/v)).

Material Characterization

Scanning electron microscopy (SEM) with a REGULUS8230 instrument was employed to characterize gel polymer electrolytes and Energy Dispersive X-ray spectroscopy (EDS) analysis was conducted to determine the samples' elemental composition and distribution.

The changes in functional group during the formation of gel polymer electrolytes were analysed using Fourier-transform infrared spectroscopy (FTIR). The FTIR instrument used was a Thermo Fisher Nicolet iS50 ATR spectrometer, with the resolution of 4 cm⁻¹.

X-ray diffraction (XRD) measurements were performed to characterize the crystal structure and phase composition of gel polymer electrolyte materials. The machine used was an EMPYREAN X-ray diffractometer, Cu $\text{K}\alpha$ ($\lambda = 1.5416 \text{ \AA}$) radiation, a 2θ ranging from 10° to 80°, and a scan rate of 0.02° s⁻¹.

Thermal analysis included both differential scanning calorimetry (DSC) and thermogravimetric analysis (TGA). DSC measurements were conducted using a NETZSCH DSC 200 F3 instrument with N_2 flow (50 mL min⁻¹), a ramp rate of 5 K min⁻¹, and a temperature range from -40 to 200°C.

The thermal stability of the gel polymer electrolytes was investigated using TGA with a NETZSCH STA 2500 instrument. Tests were carried out in an air atmosphere with a heating rate of 10 °C min⁻¹.

Electrochemical Measurements

Electrochemical impedance spectroscopy (EIS) measurements were conducted using the Multi Autolab M204 electrochemical workstation. The electrolyte was processed into small discs with a diameter of 0.6 mm and sandwiched between two stainless steel (SS) blocking electrodes. The frequency varied from 1 Hz to 1 MHz. The EIS measurement temperature was set from room temperature to 90 °C with a step of 10 °C. The ionic conductivity was obtained using the following equation:

$$\sigma = \frac{d}{RS}$$

Where d is the thickness of the gel polymer electrolyte, R is the resistance value of the bulk electrolyte, and S is the contact area between two electrolytes.

The electrochemical stability windows of gel polymer electrolytes were measured by linear sweep voltammetry (LSV). The test, conducted at a scan rate of 0.5 mV s⁻¹, was performed at room temperature from 1 V to 5 V with an $\text{Mg}|\text{SPE}|\text{SS}$ (SS: stainless steel) cell with an electrochemical workstation (DH7000, Donghua, China).

2. Results and Discussion

Figure 1 presents the morphological variations in the polymer matrix at different PPC weight ratios. The pure PVDF film appears smooth and nonporous. However, with the introduction of PPC, a porous structure is formed. This is attributed to polymers arranging themselves during phase separation, creating regions with interconnected pathways resembling pores. This phenomenon can be explained by the fact that PVDF segments, due to their crystalline structure, arrange themselves in an orderly manner, while PPC, being an amorphous polymer, forms small nuclei. The introduction of PPC into PVDF disrupts

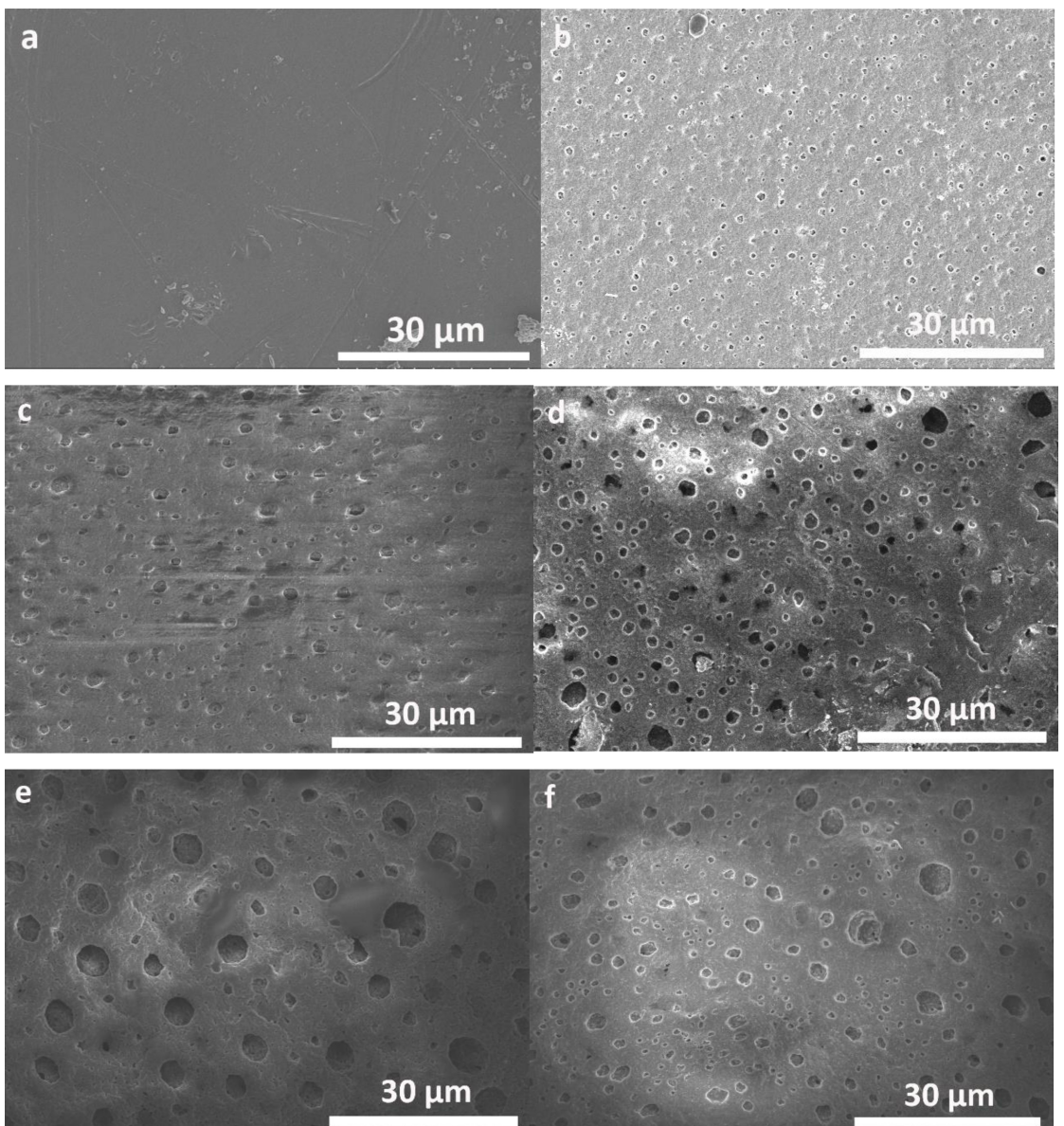


Figure 1. SEM images of the polymer matrix. (a) PVDF; (b) PVDF/10wt%PPC; (c) PVDF/20wt%PPC; (d) PVDF/30wt%PPC; (e) PVDF/40wt%PPC; (f) PVDF/50wt%PPC.

the original orderly structure, resulting in the formation of a porous structure. This structure can generate multiple channels for ionic transport, provided a pathway for the movement of Mg^{2+} ions. The average pore sizes are calculated of polymer matrix and results are included in Table 1. The systematic manual point count method (ASTM E562-11 standard) was adapted for measuring the pore sizes. As the PPC content increases from 0 wt% to 40 wt%, the average pore size increases from 0 to $3.67 \pm 1.24 \mu\text{m}$. However, the pore size of

the polymer film decreases when the PPC content reaches 50 wt%. Additionally, the pore size distribution of PVDF/50wt% PPC is not as homogeneous as the other four PVDF/PPC films. The discrepancy may be due to the high PPC content, leading to partial PPC agglomeration, as PVDF cannot be homogeneously dissolved with PPC.

Figure 2.1 shows the FTIR spectra of pure PVDF and PVDF/PPC blended polymers, and Figure 2.2 presents a partial enlargement image of FTIR curves. In the spectra, characteristic

Table 1. Average pore size of six different polymer electrolytes.

PPC (wt%)	0	10	20	30	40	50
Pore diameter (μm)	0	0.77 ± 0.23	1.56 ± 0.49	1.71 ± 0.37	3.67 ± 1.24	2.70 ± 1.38

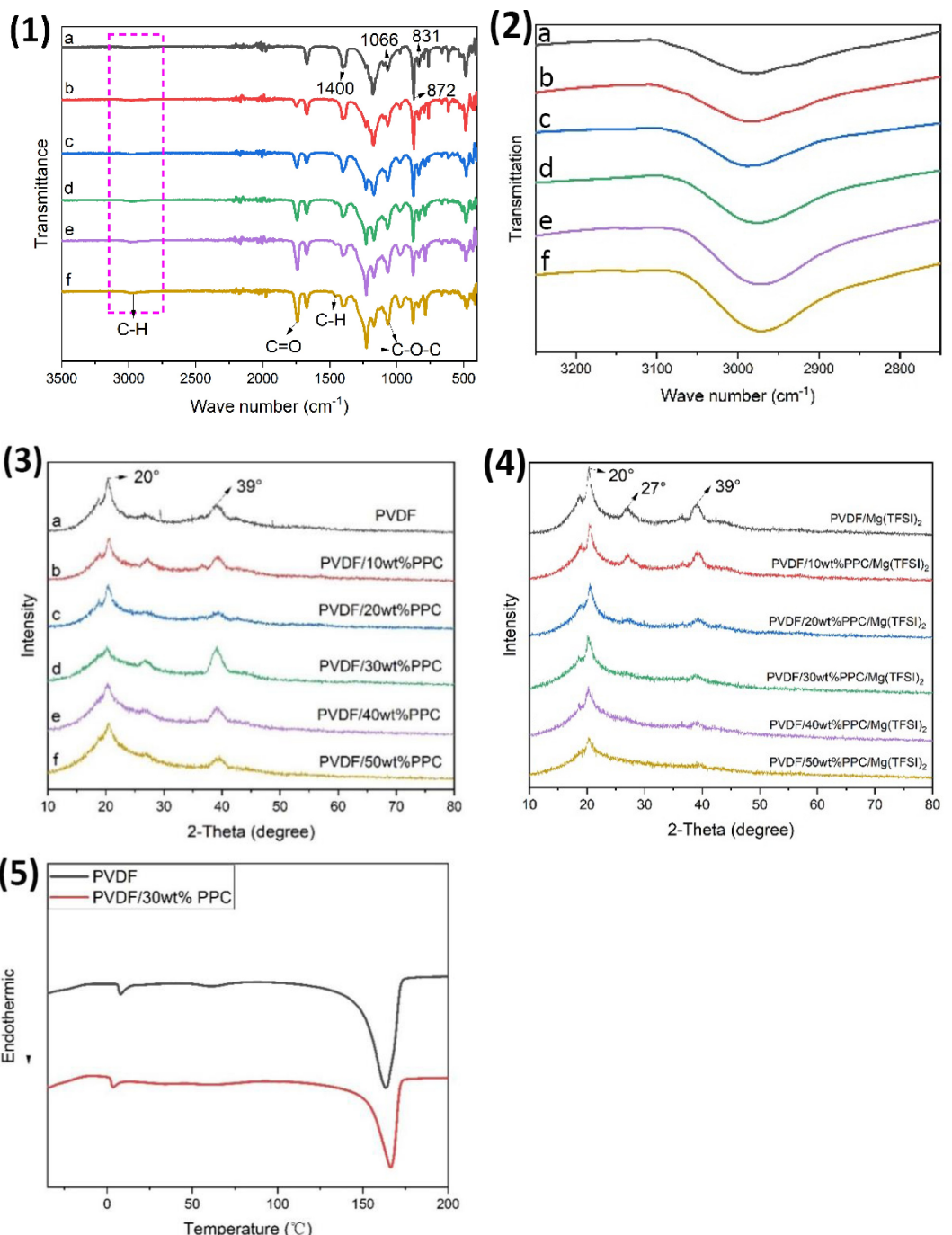


Figure 2. (1) FTIR spectra of pure PVDF and blended PVDF/PPC membranes. (2) Partial enlargement image of FTIR spectra. (3) XRD patterns of pure PVDF and blended PVDF/PPC membranes. (4) XRD patterns of pure PVDF and blended PVDF/PPC/Mg(TFSI)₂ membrane. (a) PVDF, (b) PVDF/10wt%PPC, (c) PVDF/20wt%PPC, (d) PVDF/30wt%PPC, (e) PVDF/40wt%PPC, (f) PVDF/50wt%PPC. (5) DSC curves of the PVDF and PVDF/30wt%PPC polymer matrix.

absorption peaks of PPC were identified at specific wavelengths: 3100–2800 cm⁻¹ (related to C–H stretching in CH₂ and CH₃), 1739 cm⁻¹ (C=O stretching vibration band), 1455 cm⁻¹ (C–H bending in CH₂), and 1228 and 1065 cm⁻¹ (C–O–C stretching vibration band). PVDF displays its characteristic peaks at 1400 cm⁻¹ (–CH₂– bending vibration band), 1066 cm⁻¹ (C–C stretching band), 872 cm⁻¹ (amorphous phase band), and 831 cm⁻¹ (–CH₂– bending vibration band). All the characteristic peaks of PVDF and PPC in the polymer composite films are

exhibited in the FTIR spectra, indicating the successful preparation of the polymer matrix. Furthermore, the intensity of characteristic peaks of PPC, C–H, C=O, and C–O–C, increases with the rise of the PPC content.

Figure 2.3 illustrates the blended PVDF/PPC polymers and pure PVDF polymer matrix. The pure PVDF matrix exhibits two characteristic peaks at $2\theta = 20^\circ$ and 39° , indicating the crystallization of pure PVDF. PPC is amorphous, while PVDF is crystalline, leading to phase separation to some extent. With

the introduction of PPC, the diffraction peak position remains almost the same, but the peak gets broadened, indicating reduced crystallinity. The broadening peak suggests an interaction between PVDF and PPC, possibly involving a chemical reaction. Hence, increasing the amorphous phase is beneficial for the transfer of Mg^{2+} . After immersing the polymer matrix in the liquid electrolytes to form gel polymer electrolytes, Figure 2.4 shows that the position of diffraction peaks does not change, but the relative intensities of the characteristic peaks at $2\theta = 20^\circ, 39^\circ$ become weaker. Additionally, the intensity of diffraction peaks at $2\theta = 27^\circ$ decreases and even disappears. This suggests a chemical connection between the organic liquid $Mg(TFSI)_2/EC/DEC$ and the polymers (PVDF, or PVDF/PPC). Additionally, it is observed that the crystallinity of the gel polymer electrolytes is further reduced. XRD results are consistent with DSC results. In summary, the gel polymer electrolyte is mainly amorphous due to the addition of liquid electrolytes, indicating a possible molecular-level blending of organic liquid electrolytes with the PVDF/PPC matrix.

The impact of blending PPC on the crystallinity of PVDF was further investigated through thermal analysis. Figure 2.5 shows the DSC thermograms of pure PVDF and PVDF/30wt%PPC. The crystallinity of the samples was calculated according to equation below.

$$X_c(\%) = \frac{\Delta H_m^{\text{sample}}}{\Delta H^*} \times 100\%$$

Where X_c is the crystallinity, $\Delta H_m^{\text{sample}}$ represents the enthalpy of fusion of the polymer samples, and ΔH^* is the enthalpy of fusion for 100% crystalline PVDF, 104.7 J g^{-1} .

The calculated enthalpy and crystallinity results are listed in Table 2. The melting enthalpies of PVDF decreases with the addition of PPC. The crystallinity of PVDF polymeric chains also reduced from 58.3% to 38.6% with the addition of 30wt%PPC. Furthermore, the SEM results show that incorporating PPC changed the polymer chain formation, leading to the formation of porous structure.

The electrolyte uptake can be calculated by the formula shown below:

$$\eta = \frac{w_1 - w_0}{w_0}$$

η is the electrolyte uptake (%) of different polymer membranes; w_0 , w_1 represent weights of samples before and after soaking in the liquid electrolytes, respectively.

Table 2. Calculated crystallinity of the PVDF and PVDF/PPC matrix.

Samples	Melting point Tm (°C)	Melting enthalpy $\Delta H_m (\text{J g}^{-1})$	Crystallinity $X_c (\%)$
PVDF	163.29	61.02	58.3
PVDF/30wt %PPC	166.39	40.39	38.6

EDS results in Table 3. show that the concentration of both Mg and S elements increase as the PPC content increases from 0 wt% to 30 wt%. The composition of Mg increases from 0.2 at.% to 1.06 at.%, intensifying more than fivefold. The percentage of S rises from 0.74% to 2.76%. However, when PPC content reaches 40 wt%, the concentrations of Mg and S elements are almost the same as their compositions in PVDF/30wt%PPC/Mg(TFSI)₂. This result indicates that Mg(TFSI)₂ salt in the polymer segment has reached saturation. As indicated in Figure 3, the pore size of PVDF/PPC polymer increases when the concentration of PPC increases from 0 wt% to 30 wt%. The increase in pore size facilitates the interaction between Mg^{2+} and polymer bonds, specifically the $-F-$ and $=O$ groups. From Table 4, it can be seen that there is a significantly increase of liquid uptake from 34% to 155% as the addition of PPC content from 20 wt% rise to 30 wt%. It is aligned with the trend of increasing ionic conductivity, indicating that the rise amount of soaking liquid electrolytes is beneficial for enhancing ionic conductivity of gel polymer electrolytes. More liquid electrolytes amount provides higher magnesium ion concentration.

TGA curves of pure PVDF and PVDF/30wt%PPC/Mg(TFSI)₂ gel polymer electrolytes are shown in Figure 4.1 and 4.2. The gel polymer electrolyte shows a slightly weight loss of about 5 wt% when temperature reaches about 90 °C, likely attributed to surface-adsorbed moisture. Subsequently, there is a substantial weight loss due to the evaporation of EC and DEC solvents. At around 250 °C, there is a significant weight loss in the PVDF/30wt%PPC/Mg(TFSI)₂ polymer matrix attributing to $-C=O$ decomposition. Following this reaction is the decomposition of $-C-F$ between 400 °C and 550 °C. Above 550 °C, the quality of the residue stabilizes, leaving magnesium salts that are challenging to decompose. Additionally, the residual product mass increases with the addition of 30 wt% PPC. This

Table 3. EDS analysis of different samples.

Samples	Atomic percent (%)				
	C	O	F	Mg	S
a	66.17	6.29	26.59	0.20	0.74
b	62.33	6.92	29.41	0.25	1.09
c	64.32	8.53	25.22	0.41	1.52
d	60.87	7.07	28.24	1.06	2.76
e	68.91	7.42	19.96	0.95	2.76

Table 4. A list of the electrolyte uptake amount and weights of polymer samples before and after soaking.

Samples	w_0/g	w_1/g	$\eta/\%$
PVDF	0.0243	0.0349	43%
PVDF/10wt %PPC	0.0168	0.0224	33%
PVDF/20wt %PPC	0.0156	0.0209	34%
PVDF/30wt %PPC	0.0180	0.0459	155%
PVDF/40wt %PPC	0.0550	0.1448	163%
PVDF/50wt %PPC	0.0604	0.1708	183%

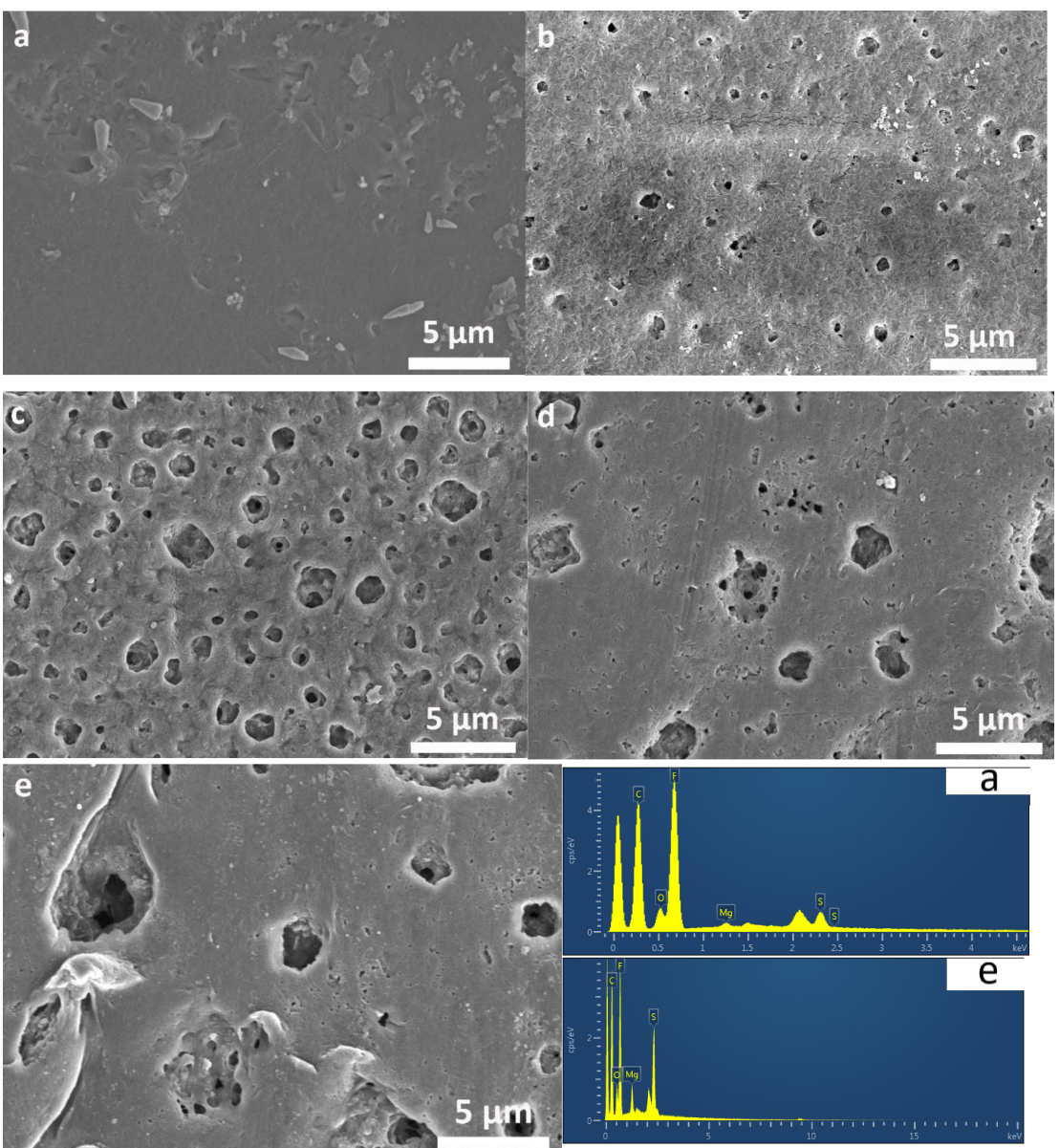


Figure 3. SEM images & EDS results of gel polymer electrolytes: (a) PVDF/Mg(TFSI)₂; (b) PVDF/10wt%PPC/Mg(TFSI)₂; (c) PVDF/20wt%PPC/Mg(TFSI)₂; (d) PVDF/30wt%PPC/Mg(TFSI)₂; (e) PVDF/40wt%PPC/Mg(TFSI)₂.

can be explained by the microporous structure absorbing more magnesium ions, and the increased magnesium ion concentration providing more free magnesium ions, enhancing ionic conductivity of gel polymer electrolytes.

The value of bulk resistance of different gel polymer electrolytes can be obtained from Figure 4.3. It can be seen that when PPC is introduced into PVDF, the bulk resistance of gel polymer electrolytes decreased significantly, which is beneficial for enhancing ionic conductivities of gel polymer electrolytes. Figure 4.4 illustrates the relationship between ionic conductivity and the temperature of PVDF/PPC/Mg(TFSI)₂ based polymer electrolytes, fitting with the Arrhenius plot of conductivity. This shows that the conductivity is thermally activated, except for the high-temperature region of the PVDF/40wt%PPC/Mg(TFSI)₂ polymer electrolyte. The Arrhenius equation is shown below:

$$\sigma = \sigma_0 \exp\left(\frac{-E_a}{kT}\right)$$

Where E_a is the activation energy, σ_0 is a pre-exponential factor and k is Boltzmann constant.

The SEM results confirm that a porous structure is formed with the addition of PPC into PVDF, providing a pathway for fast Mg²⁺ ion transport. In other words, the microporous structure is beneficial for increasing the ionic conductivities of GPEs. There are two Mg ion transport pathways. The first pathway involves magnesium ions coordinating with fluorine and ester atoms on the polymer chain when the polymer matrixes are immersed in organic liquid electrolytes. Ions experience a coordination-dissociation process with the electron-donating groups at different positions with the thermal

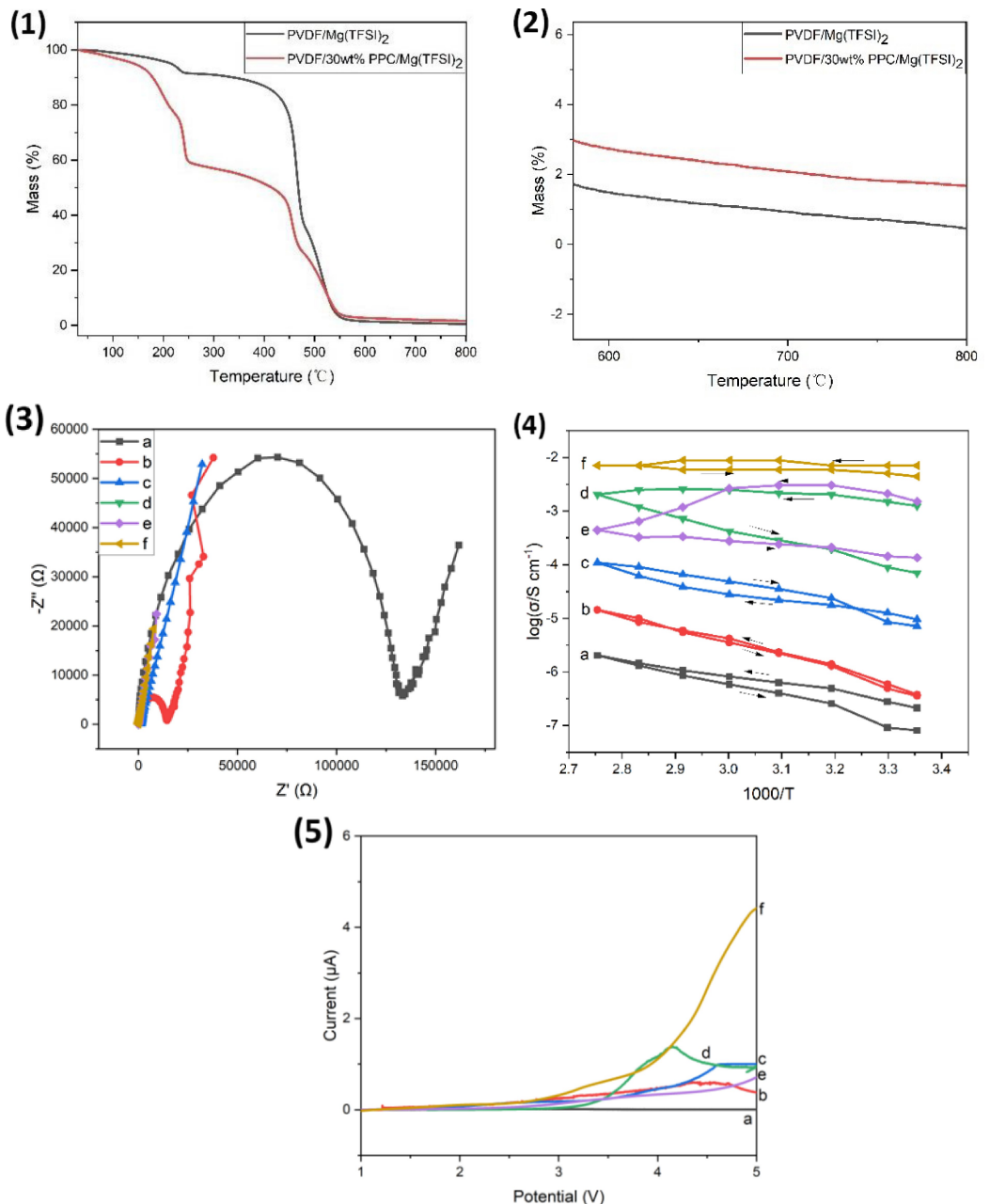


Figure 4. (1) TGA curves of PVDF/Mg(TFSI)₂ film and PVDF/30wt%PPC/Mg(TFSI)₂ polymer electrolyte film. (2) Partial enlargement images of TGA curves. (3) Nyquist plots of the six samples at room temperatures. (4) The relationship between ionic conductivity and temperature across various samples within the range of 25°C to 90°C. (5) Linear sweep voltammogram of six polymer electrolytes. (a) PVDF/Mg(TFSI)₂; (b) PVDF/10wt%PPC/Mg(TFSI)₂; (c) PVDF/20wt%PPC/Mg(TFSI)₂; (d) PVDF/30wt%PPC/Mg(TFSI)₂; (e) PVDF/40wt%PPC/Mg(TFSI)₂; (f) PVDF/50wt%PPC/Mg(TFSI)₂.

motion of the molecular chain to achieve ion conduction. The second pathway is that magnesium ions can move forward with molecular motion in the liquid as the polymer electrolyte contains a trace amount of organic solvent as the plasticizer. Figure 4.4 displays that the second pathway contributes more to ion conduction, exhibiting the properties of gel polymer electrolyte ion conduction. It also illustrates the ionic conductivity of those polymer electrolytes remains almost unchanged before and after heating and cooling, indicating that the electrolytes possess good thermal stability. The ionic conductivity increases at room temperature with the increase in

PPC content. Notably, there is a sharp increase in ionic conductivity from 10^{-7} to 10^{-3} S cm⁻¹ when the concentration of PPC increases from 0 wt.% to 30 wt.%. Table 5 exhibits ionic conductivities of different types of PVDF-based polymer electrolytes, ethylene carbonate and ether as plasticizer. It shows that prepared gel polymer electrolytes have a high ionic conductivity at room temperature and good electrochemical stability window.

Figure 4.5 shows the linear sweep voltammetry results of six gel polymer electrolytes. No reaction peak is observed up to 3 V compared to Mg²⁺/Mg for all GPE samples. The anodic current

Table 5. Ionic conductivity of PVDF-PPE–Mg(TFSI)₂ based electrolyte and other gel polymer electrolytes.

Composition	Conductivity (S cm ⁻¹)	Temp.	Ref.
PEO-PMA–Mg[(CF ₃ SO ₂) ₂ N] ₂ –EC–DMC (carbonate-based)	2.8×10 ⁻³	RT	[10a]
PEO-PMA–Mg[(CF ₃ SO ₂) ₂ N] ₂ –PEGDE (ether-based)	10 ⁻⁴	20	[10b]
PEO-PVDF–Mg[(CF ₃ SO ₂) ₂ N] ₂	1.2×10 ⁻⁵	25	[17]
PVDF-MgTr-PC-EC (carbonated-based)	2.67×10 ⁻³	20	[18]
PMMA–Mg(CF ₃ SO ₃) ₂ –EC–DEC (carbonated-based)	5.58×10 ⁻⁵	RT	[14]
PVDF-PPC–Mg(TFSI) ₂ –EC–DEC (carbonated-based)	5×10 ⁻³	25	This work

of sample (a), PVDF/Mg(TFSI)₂, remains near zero as the potential increases from 1 V to 5 V. However, as the concentration of PPC increases from 10% to 50%, the anodic current significantly rises within the voltage range of 3 V to 5 V. These LSV results demonstrate that the gel polymer electrolyte exhibits good anodic stability within the operational potential range of 1.0 V to 3.0 V. It possesses an electrochemical stability window equal to that of the all-phenyl complex (APC) liquid electrolyte (3.0 V).^[7a] PVDF contains –C–F groups with fluorine atoms and a high dielectric constant of $\epsilon=8.4$,^[19] and Mg(TFSI)₂ has a relatively low dissociation energy. When Mg(TFSI)₂ salts interact with F–C and C=O functional groups, they can be separated into Mg²⁺ cations and TFSI⁻ anions and cannot recombine together. Since TFSI⁻ anions have larger steric hindrance, Mg²⁺ ions have greater freedom to transport through the polymer matrix. As a result, this enhances the capability for magnesium ion transfer. The schematic diagram in Figure 5 illustrates the transport pathway of magnesium ions in the polymer electrolytes. The magnesium ions can coordinate and dissociation with fluorine atoms and –O– functional groups and achieve conduction with the thermal motion of molecular chains.

3. Conclusions

The experimental results show that the amorphous phase improves the transport of magnesium ions in the polymer. This research has synthesized a series of PVDF/PPC-based solid state electrolytes, with the PVDF/30wt%PPC/Mg(TFSI)₂ electrolyte demonstrating the highest ionic conductivity at 10⁻³ S cm⁻¹. The addition of PPC into PVDF forms a microporous structure,

combining with Mg(TFSI)₂ salt to provide a pathway for fast Mg²⁺ ion transport. This is beneficial for enhancing the ionic conductivities of GPEs. Both XRD and DSC results illustrate that the crystallinity of PVDF/PPC polymer matrix decreased as the PPC content increased, indicating that addition of an appropriate amount of PPC can manipulate the crystalline phase of PVDF, forming a microporous structure. This research demonstrates a pathway to improve the Mg²⁺ ionic conductivity of polymer-based solid-state electrolyte at room temperature. Selecting suitable negative and positive electrode materials would promote the design and development of magnesium-based all-solid-state rechargeable batteries at room temperature.

Acknowledgements

Dr Shanghai Wei wishes to thank the Ministry of Business, Innovation & Employment (MBIE), New Zealand, for the Smart Ideas Grant via project No. UOAX 2210. Dr Yigang Yan acknowledges the supported by the National Natural Science Foundation of China (No.21975168), Sichuan Science and Technology Program (2021JDJQ0020). Jiawei Liu is thankful for the scholarship from the China Scholarship Council (No.202109110063). Open Access publishing facilitated by The University of Auckland, as part of the Wiley - The University of Auckland agreement via the Council of Australian University Librarians.

Conflict of Interests

The authors declare no competing financial interest.

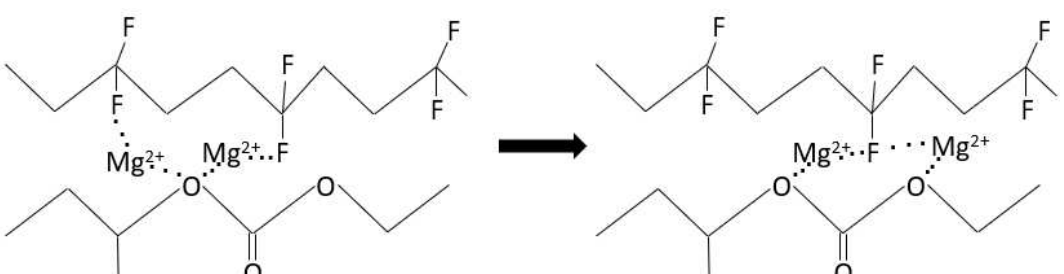


Figure 5. Schematic illustration of main interaction between polymer and ions in the GPE.

Data Availability Statement

The data that support the findings of this study are available from the corresponding author upon reasonable request.

Keywords: Gel polymer electrolyte · high ionic conductivity · polymer · magnesium battery · rechargeable batteries

- [1] a) Z. Li, Y. X. Yao, S. Sun, C. B. Jin, N. Yao, C. Yan, Q. Zhang, *Angew. Chem. Int. Ed. Engl.* **2023**, *62*, e202303888; b) L. Zhang, C. Zhu, S. Yu, D. Ge, H. Zhou, *J. Energy Chem.* **2022**, *66*, 260–294; c) H. Zhou, J. Xie, L. Bao, S. Qiao, J. Sui, J. Wang, *J. Energy Chem.* **2022**, *73*, 360–369; d) Z. Song, X. Wang, H. Wu, W. Feng, J. Nie, H. Yu, X. Huang, M. Armand, H. Zhang, Z. Zhou, *Journal of Power Sources Advances* **2022**, *14*; 100088e) Y. Jin, X. Zong, X. Zhang, Z. Jia, H. Xie, Y. Xiong, *Energy Storage Mater.* **2022**, *49*, 433–444.
- [2] a) D. Aurbach, Z. Lu, A. Schechter, Y. Gofer, H. Gizbar, R. Turgeman, Y. Cohen, M. Moshkovich, E. Levi, *Nature* **2000**, *407*, 724–727; b) H. D. Yoo, I. Shterenberg, Y. Gofer, G. Gershinsky, N. Pour, D. Aurbach, *Energy Environ. Sci.* **2013**, *6*, 2265–2279; c) J. Muldoon, C. B. Bucur, T. Gregory, *Chem. Rev.* **2014**, *114*, 11683–11720.
- [3] I. Shterenberg, M. Salama, Y. Gofer, E. Levi, D. Aurbach, *MRS Bull.* **2014**, *39*, 453–460.
- [4] a) F. Liu, T. Wang, X. Liu, L. Z. Fan, *Adv. Energy Mater.* **2020**, *11*, 2000787; b) P. Saha, M. K. Datta, O. I. Velikokhatnyi, A. Manivannan, D. Alman, P. N. Kumta, *Prog. Mater. Sci.* **2014**, *66*, 1–86.
- [5] Z. Liang, C. Ban, *Angew. Chem. Int. Ed. Engl.* **2021**, *60*, 11036–11047.
- [6] R. Deivanayagam, B. J. Ingram, R. Shahbazian-Yassar, *Energy Storage Mater.* **2019**, *21*, 136–153.
- [7] a) H. Shuai, J. Xu, K. Huang, *Coord. Chem. Rev.* **2020**, *422*; b) Y. Shao, N. N. Rajput, J. Hu, M. Hu, T. Liu, Z. Wei, M. Gu, X. Deng, S. Xu, K. S. Han, J. Wang, Z. Nie, G. Li, K. R. Zavadil, J. Xiao, C. Wang, W. A. Henderson, J.-G. Zhang, Y. Wang, K. T. Mueller, K. Persson, J. Liu, *Nano Energy* **2015**, *12*, 750–759.
- [8] X. Huang, S. Zeng, J. Liu, T. He, L. Sun, D. Xu, X. Yu, Y. Luo, W. Zhou, J. Wu, *J. Phys. Chem. C* **2015**, *119*, 27882–27891.
- [9] a) A. Du, H. Zhang, Z. Zhang, J. Zhao, Z. Cui, Y. Zhao, S. Dong, L. Wang, X. Zhou, G. Cui, *Adv. Mater.* **2019**, *31*, e1805930; b) N. Yoshimoto, T. Shirai, M. Morita, *Electrochim. Acta* **2005**, *50*, 3866–3871; c) R. Deivanayagam, M. Cheng, M. Wang, V. Vasudevan, T. Foroozan, N. V. Medhekar, R. Shahbazian-Yassar, *ACS Appl. Energ. Mater.* **2019**, *2*, 7980–7990; d) T. Wang, X. Zhao, F. Liu, L.-Z. Fan, *J. Energy Chem.* **2021**, *59*, 608–614.
- [10] a) N. Yoshimoto, S. Yakushiji, M. Ishikawam, M. Morita, *Electrochim. Acta* **2003**, *48*, 2317–2322; b) H. N. M. Sarangika, M. A. K. L. Dissanayake, G. K. R. Senadeera, R. R. D. V. Rathnayake, H. M. J. C. Pitawala, *Ionics* **2016**, *23*, 2829–2835.
- [11] a) G. G. Kumar, N. Munichandraiah, *J. Power Sources* **2001**, *102*, 46–54; b) Nidhi, S. Patel, R. Kumar, *J. Alloys Compd.* **2019**, *789*, 6–14.
- [12] J. Sun, Y. Zou, S. Gao, L. Shao, C. Chen, *ACS Appl. Mater. Interfaces* **2020**, *12*, 54711–54719.
- [13] R. Manjuladevi, M. Thamilselvan, S. Selvasekarpandian, P. Christopher Selvin, R. Mangalam, S. Monisha, *Ionics* **2017**, *24*, 1083–1095.
- [14] S. N. Asmara, M. Z. Kufian, S. R. Majid, A. K. Arof, *Electrochim. Acta* **2011**, *57*, 91–97.
- [15] R. Prasanth, N. Shubha, H. H. Hng, M. Srinivasan, *J. Power Sources* **2014**, *245*, 283–291.
- [16] a) Pravin N. Didwal, Y. N. Singhbabu, R. Verma, B.-J. Sung, G.-H. Lee, J.-S. Lee, D. R. Chang, C.-J. Park, *Energy Storage Mater.* **2021**, *37*, 476–490; b) L. Zhu, P. Zhu, S. Yao, X. Shen, F. Tu, *Int. J. Energy Res.* **2019**, *43*, 4854–4866.
- [17] R. Rathika, S. A. Suthanthiraraj, *Macromol. Res.* **2016**, *24*, 422–428.
- [18] G. G. Kumar, N. Munichandraiah, *J. Power Sources* **2001**, *102*, 46–54.
- [19] H. Aziam, B. Larhrib, C. Hakim, N. Sabi, H. Ben Youcef, I. Saadoune, *Renewable Sustainable Energy Rev.* **2022**, *167*, 112694.

Manuscript received: January 24, 2024

Revised manuscript received: April 17, 2024

Accepted manuscript online: April 24, 2024

Version of record online: June 3, 2024